

Application of Clumpy Torus Model to Broadband X-ray Spectra of Two Seyfert 1 Galaxies: IC 4329A and NGC 7469

SHOJI OGAWA,¹ YOSHIHIRO UEDA,¹ SATOSHI YAMADA,¹ ATSUSHI TANIMOTO,¹ AND TOSHIHIRO KAWAGUCHI²

¹*Department of Astronomy, Kyoto University, Kitashirakawa-Oiwake-cho, Sakyo-ku, Kyoto 606-8502, Japan*

²*Department of Economics, Management and Information Science, Onomichi City University, Hiroshima 722-8506, Japan*

(Received 2019 February 4; Revised 2019 March 2; Accepted 2019 March 6)

ABSTRACT

We apply a new X-ray clumpy torus model called XCLUMPY (Tanimoto et al. 2019), where the clump distribution is assumed to be the same as in the infrared clumpy torus model (CLUMPY) by Nenkova et al. (2008a,b), to the broadband X-ray spectra of type-1 active galactic nuclei (AGNs) for the first time. We analyze the archival data of IC 4329A and NGC 7469 observed with *NuSTAR/Suzaku* and *NuSTAR/XMM-Newton*, respectively, whose infrared spectra were studied with CLUMPY by Ichikawa et al. (2015) and optical extinctions (A_V) of the tori were estimated. We consider two models, invoking (Model 1) a relativistic reflection component from the accretion disk and (Model 2) a partial absorber. Assuming that the narrow Fe K α emission line at 6.4 keV originates from the torus, we separate the contribution of the torus reflection components in the total spectra. Our models yield equatorial hydrogen column densities of the tori to be $N_{\text{H}}^{\text{Equ}} = (0.53\text{--}1.43) \times 10^{23} \text{ cm}^{-2}$ and $N_{\text{H}}^{\text{Equ}} = (0.84\text{--}1.43) \times 10^{24} \text{ cm}^{-2}$, for IC 4329A and NGC 7469, respectively. We find that the N_{H}/A_V ratios in the tori are by factors of 25–68 (IC 4329A) and 2.4–3.9 (NGC 7469) smaller than that in the Galactic interstellar medium (ISM). These results suggest that a non-negligible fraction of AGNs are “dust-rich” compared with the Galactic ISM, as opposite to the general trend previously reported in many obscured AGNs.

Keywords: X-rays: galaxies – galaxies: Seyfert – galaxies: individual (IC 4329A, NGC 7469)

1. INTRODUCTION

To reveal basic properties of obscuring material in active galactic nuclei (AGNs), often referred as the “torus”, is important to understand feeding and feedback mechanisms of AGNs (see e.g., Ramos Almeida & Ricci 2017, for a recent review). Among them, the gas-to-dust ratio is a key parameter to understand the circumnuclear environments. It has been reported in many (but not all) AGNs that the ratios of optical extinction (A_V) to hydrogen column density (N_{H}) toward the nuclei, as estimated from the infrared/optical and X-ray spectra, respectively, are smaller than the Galactic value (Maiolino et al. 2001; Vasudevan et al. 2009; Bartscher et al. 2016). A plausible explanation is that the gas-to-dust ratio of obscuring material is higher (i.e., more “gas rich”) than that of the Galactic interstellar medium (ISM). It may be due to dust-free neutral gas in the broad line region (BLR), which can also cause variability in the X-ray absorption (see Bartscher et al. 2016 and references therein). However, opposite cases (i.e., torus is more “dust-rich” than Galactic) have also been

reported (e.g., Barcons et al. 2003; Huang et al. 2011; Ordovás-Pascual et al. 2017), making our understanding of AGN environments not that simple. More independent studies using a well studied, local AGN sample are necessary to solve this issue.

The X-ray spectrum of an AGN contains a reflection component from the torus, accompanied by narrow fluorescence lines such as Fe K α at 6.4 keV. This component carries information of all material *including gas and dust* around the supermassive black holes (SMBH). In particular, even in type-1 AGNs where no line-of-sight absorption is observed, the equivalent width of the Fe K α line can be used to infer the torus structure, such as its covering fraction and/or column density (e.g., Tazaki et al. 2013; Kawamuro et al. 2016). Complementary to the X-ray data, the infrared spectra give information on the properties of *dust*. Thus, comparing the X-ray and infrared spectra is quite useful to constrain the nature of AGN tori (e.g., Ricci et al. 2014), including the gas-to-dust ratio. In such studies, it is desired to apply

“self-consistent” models in terms of the torus geometry to both X-ray and infrared data.

Recently, Tanimoto et al. (2019) have constructed a new X-ray clumpy torus model called XCLUMPY, based on the Monte Carlo simulation for Astrophysics and Cosmology (MONACO: Odaka et al. 2016) framework. In this model, the geometry of the torus is the same as that in the CLUMPY model in the infrared band (Nenkova et al. 2008a,b), where clumps are distributed according to power law and normal profiles in the radial and angular directions, respectively. It has three variable torus parameters: equatorial hydrogen column density, torus angular width, and inclination angle. The XCLUMPY model enables us to directly compare the results with those obtained from the infrared spectra with the CLUMPY code in a self-consistent way.

In this paper, we apply the XCLUMPY model to the X-ray spectra of unobscured (type-1) AGNs for the first time. Our sample is IC 4329A and NGC 7469, whose infrared spectra have been analyzed in detail with the CLUMPY model (Ichikawa et al. 2015). We utilize their best-quality broadband X-ray spectra, simultaneously observed with *NuSTAR* and *Suzaku* (for IC 4329A) and with *NuSTAR* and *XMM-Newton* (NGC 7469). This work is complementary to those for obscured AGNs that compare the line-of-sight column densities with the A_V values obtained with the CLUMPY model (González-Martín et al. 2013; Tanimoto et al., in prep.). The main goal of our paper is to constrain the torus properties, in particular the gas-to-dust ratios. In addition, we can also correctly estimate the contribution of the reflection component from the torus in the total spectra. Two major models have been proposed as the X-ray spectra of type-1 AGNs to explain the broad iron-K emission line feature and bump structure peaked around 30 keV: one invoking a relativistic reflection component from the innermost accretion disk, the other assuming variable partial absorbers (see Section 3). Although to discriminate these models is not a purpose of our paper (and hence we treat the two models equally), it is always crucial to properly take into account the torus reflection component in modeling the broadband X-ray spectra of AGNs.

This paper is organized as follows. Section 2 gives the details of our sample. In Section 3, we describe the observations and data reduction. In Section 4, we present the analysis of the broadband X-ray spectra by applying the XCLUMPY model. In Section 5, we compare our results with the previous studies and discuss their torus properties. We adopt the cosmological parameters of $(H_0, \Omega_m, \Omega_\Lambda) = (70 \text{ km s}^{-1} \text{ M pc}^{-1}, 0.3, 0.7)$ and the solar abundances of Anders & Grevesse (1989) through-

out the paper. Errors on spectral parameters correspond to 90% confidence limits for single parameters.

2. SAMPLE

For our study we selected two Seyfert 1 galaxies, IC 4329A ($z = 0.0161$; Willmer et al. 1991) and NGC 7469 ($z = 0.0163$; Springob et al. 2005), from the sample of Ichikawa et al. (2015). To constrain the torus parameters, Ichikawa et al. (2015) applied the CLUMPY model to the infrared spectral energy distributions of 21 nearby AGNs obtained with *Spitzer* and high-spatial resolution cameras on ground-based telescopes. Among them, these are the two AGNs that show low X-ray absorptions ($N_H < 10^{23} \text{ cm}^{-2}$). We excluded NGC 4151 and NGC 1365, which are classified as Seyfert 1 galaxies but are known to show very complex, variable absorption in the X-ray bands (see e.g., Yaqoob & Warwick 1991 and Risaliti et al. 2005, respectively).

The X-ray data of these sources were analyzed by many authors (e.g., for IC 4329A, Done et al. 2000 (*ASCA+RXTE*), Gondoin et al. 2001 (*XMM-Newton+BeppoSAX*), McKernan & Yaqoob 2004 (*Chandra/HETGS*), Steenbrugge et al. 2005 (*XMM-Newton*), Beckmann et al. 2006 (*INTEGRAL*), Winter et al. 2009 (*Swift/BAT*), Patrick et al. 2012 (*Suzaku+Swift/BAT*), Miyake et al. 2016 (*Suzaku*), Iso et al. 2016 (*Suzaku*) and Brenneman et al. 2014 (*Suzaku+NuSTAR*); for NGC 7469, e.g., Guainazzi et al. 1994 (*ASCA*), Nandra et al. 2000 (*RXTE*) De Rosa et al. 2002 (*BeppoSAX*), Blustin et al. 2003 (*XMM-Newton*), Scott et al. 2005 (*Chandra/HETGS*), Winter et al. 2009 (*Swift/BAT*), Patrick et al. 2012 (*Suzaku+Swift/BAT*), Iso et al. 2016 (*Suzaku*) and Midei et al. 2018 (*XMM-Newton+NuSTAR*)). The *Chandra/HETGS* observations (Shu et al. 2010) confirmed the presence of a narrow ($< 10,000 \text{ km s}^{-1}$ in FWHM) Fe $K\alpha$ component centered at 6.4 keV in both IC 4329A (see their Appendix) and NGC 7469; in IC 4329A, excess emission is detected at $\approx 6.0\text{--}6.4 \text{ keV}$, which can be interpreted as a modestly broadened Fe $K\alpha$ line from the disk (Brenneman et al. 2014). Many of these works employed the *pexrav* model (Magdziarz & Zdziarski 1995) with an Fe $K\alpha$ line, the *pexmon* model (Nandra et al. 2007), which includes self-consistently calculated fluorescence lines, or the *xillver* model (García et al. 2014) whose ionization parameter is fixed at zero, to represent the reflection component from the torus, or to approximate total reflection components including that from the accretion disk. Models of relativistic reflection from the accretion disk have been applied by Done et al. (2000) and Patrick et al. (2012) for IC 4329A, and by De Rosa et al. (2002) and Patrick et al. (2012) for

NGC 7469. Iso et al. (2016) systematically applied a partial covering model to local Seyfert galaxies including our targets.

3. OBSERVATIONS AND DATA REDUCTION

We analyze the best-quality simultaneous broadband X-ray spectra that cover the energy band from 0.3 keV to 70 keV with a CCD energy resolution below ~ 10 keV. IC 4329A was observed simultaneously with *Suzaku* (Mitsuda et al. 2007) and *NuSTAR* (Harrison et al. 2013) in 2012, and NGC 7469 was with *XMM-Newton* (Jansen et al. 2001) and *NuSTAR* in 2015. The observation log of the X-ray data used in this paper is given in Table 1. Details of data reduction are described below.

3.1. IC 4329A

3.1.1. *Suzaku*

Suzaku observed IC 4329A in 2012 August. It carried four X-ray CCD cameras (X-ray imaging spectrometer; XISs (Koyama et al. 2007)) and a non-imaging instrument (the hard X-ray detector; HXD (Takahashi et al. 2007)), which cover the energy band below and above ≈ 10 keV, respectively. XIS0, XIS2, and XIS3 are frontside-illuminated CCDs (XIS-FI) and XIS1 is the backside-illuminated one (XIS-BI). The HXD consists of the PIN (10–70 keV) and GSO (40–600 keV) detectors (Kokubun et al. 2007).

We reprocessed the unfiltered XIS event data with the AEPIPELINE script. Events were extracted from a circular region with a radius of 160 arcsec centered at the source position. The background was taken from a source-free circular region with a radius of 120 arcsec. We generated the response matrix file (RMF) with XIS-RMFGEN and ancillary response files (ARF) with XISS-MARFGEN (Ishisaki et al. 2007). To improve the statistics, we co-added the spectra of XIS0 and XIS3. The spectrum were binned to contain at least 1000 counts per bin. We did not utilize the data of XIS1, whose effective area in the iron-K band was smaller than those of XIS-FIs, to avoid cross-calibration uncertainties.

The unfiltered HXD data were also reprocessed by using AEPIPELINE. We only analyzed the PIN data, because the source was weakly detected with the GSO (Brenneman et al. 2014). We utilized the “tuned” background event files (Fukazawa et al. 2009) to make the spectrum of the non-X-ray background (NXB), to which a simulated spectrum of the cosmic X-ray background was added. In the spectral analysis, we only utilized the 16–40 keV range, where the source flux is brighter than 3% of the NXB level (the maximum systematic error in the 15–70 keV range; see Fukazawa et al. 2009).

3.1.2. *NuSTAR*

NuSTAR also observed IC 4329A in 2012 August simultaneously with the *Suzaku* observation. *NuSTAR* carries two focal plane modules (FPMs: FPMA and FPMB), which cover an energy range of 3–79 keV. We analyzed the FPMs data with HEASOFT v6.21 and CALDB released in 2017 December 12. We extracted the spectrum from a circular region with a 75 arcsec radius centered at the source peak, and took the background from a nearby source-free circular region with the same radius. We then combined the source spectra, background spectra, RMF, and ARF, using the ADDASCASPEC script. The combined spectrum was binned to contain at least 1000 counts per bin.

3.2. NGC 7469

3.2.1. *XMM-Newton*

XMM-Newton observed NGC 7469 in 2015 June. It carries three X-ray CCD cameras, one EPIC/PN (Strüder et al. 2001) and MOS (Turner et al. 2001). We analyzed only the data of PN, which has much larger effective area than the MOS detectors, using the Science Analysis Software (SAS) v17.0.0 and current calibration file (CCF) released on 2018 June 22. The PN data were reprocessed with the EPPROC script. We extracted the spectrum from a circular region with a radius of 40 arcsec centered at the source peak, and took the background from a source-free circular region with a 50 arcsec radius in the same CCD chip. We generated the RMF with RMFGEN and ARF with ARFGEN. The spectrum was binned to contain at least 100 counts per bin.

3.2.2. *NuSTAR*

NGC 7469 was also observed with *NuSTAR* in 2015 June simultaneously with *XMM-Newton*. We extracted the FPMs spectra from a circular region with a 70 arcsec radius centered at the source peak, and took the background from a nearby source-free circular region with the same radius. We combined the spectra of FPMs, using ADDASCASPEC. The combined spectrum was binned to contain at least 100 counts per bin.

4. X-RAY SPECTRAL ANALYSIS AND RESULTS

It is well established from previous studies that a typical X-ray spectrum of Seyfert 1 galaxies cannot be represented by a single power law but consists of multiple components: a direct power-law component with an exponential cutoff (or thermally Comptonized component), its reflection components from the torus and/or the accretion disk, and a soft excess (see e.g., Risaliti & Elvis 2004). Absorptions by ionized matter (warm

Table 1. Summary of Observations

Object	Satellite	ObsID	Start Date(UT)	End Date(UT)	Net Exposure(ks)
IC 4329A	<i>Suzaku</i>	707025010	2012-08-13 02:13:09	2012-08-14 10:53:03	117.6
	<i>NuSTAR</i>	60001045002	2012-08-12 16:06:07	2012-08-14 13:12:46	162.4
NGC 7469	<i>XMM-Newton</i>	0760350201	2015-06-12 13:36:49	2015-06-13 14:50:09	90.8
	<i>NuSTAR</i>	60101001002	2015-06-12 18:41:07	2015-06-13 00:40:46	21.6

Table 2. Best-fit Parameters of IC 4329A

Component	No.	Parameter	Model 1	Model 2	Units
ZXIPCF1	(1)	N_{H}	$5.68^{+0.06}_{-0.12}$	$5.92^{+0.13}_{-0.12}$	10^{21} cm^{-2}
	(2)	$\log \xi$	$0.27^{+0.01}_{-0.10}$	$0.17^{+0.10}_{-0.09}$	
ZXIPCF2	(3)	N_{H}	...	1.04 ± 0.06	10^{24} cm^{-2}
	(4)	$\log \xi$...	$1.91^{+0.06}_{-0.14}$	
	(5)	C_{frac}	...	$0.23^{+0.01}_{-0.02}$	
ZCUTOFFPL	(6)	Γ	1.77 ± 0.01	1.83 ± 0.01	
	(7)	E_{Cut}	318^{+53}_{-60}	1000^{+0}_{-115} ^a	keV
	(8)	K_{P}	$3.05^{+0.02}_{-0.03}$	$4.21^{+0.13}_{-0.14}$	$10^{-2} \text{ photon cm}^{-2} \text{ s}^{-1}$
ZGAUSS	(9)	E_{Line}	0.77 ± 0.01	0.77 ± 0.01	keV
	(10)	σ_{Line}	$2.98^{+0.27}_{-0.55}$	3.17 ± 0.58	10^{-2} keV
	(11)	K_{L}	$4.07^{+0.37}_{-0.44}$	$3.99^{+0.51}_{-0.46}$	$10^{-4} \text{ photon cm}^{-2} \text{ s}^{-1}$
RELXILL	(12)	$\log \xi$	$0.29^{+0.71}_{-0.29}$...	
	(13)	R_{in}	87^{+73}_{-31}	...	r_{G}
	(14)	R	$3.20^{+0.13}_{-0.25}$...	10^{-3}
XCLUMPY	(15)	$N_{\text{H}}^{\text{Equ}}$	$0.66^{+0.11}_{-0.13}$	$1.35^{+0.08}_{-0.09}$	10^{23} cm^{-2}
	(16)	σ	40 (fixed)	40 (fixed)	degree
	(17)	i^{b}	18.19 (fixed)	18.19 (fixed)	degree
	(18)	C_{NuSTAR}	0.97 ± 0.01	0.97 ± 0.01	
	(19)	L_{2-10}	6.47	8.14	$10^{43} \text{ erg s}^{-1}$
		χ^2/dof	1338.8/1120	1321.2/1120	

NOTE— (1) Hydrogen column density of a full absorber. (2) Its logarithmic ionization parameter, ξ (erg cm s^{-1}). (3) Hydrogen column density of a partial absorber. (4) Its logarithmic ionization parameter. (5) Its covering fraction. (6) Photon index. (7) Cutoff energy. (8) Power-law normalization of the direct component. (9) Energy of the emission line. (10) Line width of the emission line. (11) Normalization of the emission line. (12) Logarithmic ionization parameter of the accretion disk. (13) The inner radius of the disk. (14) Reflection strength. (15) Torus hydrogen column density along the equatorial plane. (16) Torus angular width. (17) Inclination angle. (18) Cross-calibration constant of *NuSTAR* relative to *Suzaku*/XIS. (19) Intrinsic luminosity in the 2–10 keV.

^aThe upper limit is pegged at the upper boundary value in the table model.

^bBecause the infrared result ($i = 4^{+4}_{-3}$ degrees) is out of the allowed range of XCLUMPY, we fix it at its lower limit (18.19 degrees); differences from $i = 4$ degrees are expected to be negligible (Tanimoto et al. 2019).

Table 3. Best-fit parameters of NGC 7469

Component	No.	Parameter	Model 1	Model 2	Units
ZXIPCF1	(1)	N_{H}	$1.30^{+0.15}_{-0.20}$	$1.56^{+0.13}_{-0.14}$	10^{21} cm^{-2}
	(2)	$\log \xi$	2.49 ± 0.06	2.40 ± 0.05	
ZXIPCF2	(3)	N_{H}	...	$1.80^{+0.22}_{-0.21}$	10^{24} cm^{-2}
	(4)	$\log \xi$...	$3.18^{+0.22}_{-0.14}$	
	(5)	C_{frac}	...	0.15 ± 0.04	
ZCUTOFFPL	(6)	Γ	$1.92^{+0.06}_{-0.04}$	$1.84^{+0.04}_{-0.02}$	
	(7)	E_{Cut}	$322^{+678\text{a}}_{-122}$	$321^{+679\text{a}}_{-139}$	keV
	(8)	K_{P}	$9.22^{+0.96}_{-0.60}$	$8.90^{+1.04}_{-0.63}$	$10^{-3} \text{ photon cm}^{-2} \text{ s}^{-1}$
COMPTT	(9)	T_{bb}	$8.10^{+0.74}_{-0.35}$	$8.61^{+0.18}_{-0.12}$	10^{-2} keV
	(10)	T_{P}	$2.40^{+1.71}_{-2.40}$	$9.60^{+2.28}_{-1.09}$	keV
	(11)	τ	$3.21^{+0.56}_{-0.46}$	$1.04^{+0.18}_{-0.14}$	
	(12)	K_{S}	$1.68^{+0.57}_{-0.81}$	$5.11^{+9.65}_{-0.81}$	$10^{-2} \text{ photon cm}^{-2} \text{ s}^{-1}$
RELXILL	(13)	$\log \xi$	$0.99^{+0.75}_{-0.26}$...	
	(14)	R_{in}	$9.4^{+26}_{-3.4}$...	r_{G}
	(15)	R	$2.64^{+0.23}_{-0.50}$...	10^{-3}
XCLUMPY	(16)	$N_{\text{H}}^{\text{Equ}}$	$1.00^{+0.32}_{-0.17}$	$1.00^{+0.43}_{-0.16}$	10^{24} cm^{-2}
	(17)	σ	21 (fixed)	21 (fixed)	degree
	(18)	i	59 (fixed)	59 (fixed)	degree
	(19)	C_{NuSTAR}	1.13 ± 0.01	1.13 ± 0.01	
	(20)	L_{2-10}	1.68	1.83	$10^{43} \text{ erg s}^{-1}$
		χ^2/dof	1668.7/1576	1683.6/1576	

NOTE— (1) Hydrogen column density of a full absorber. (2) Its logarithmic ionization parameter, ξ (erg cm s^{-1}). (3) Hydrogen column density of a partial absorber. (4) Its logarithmic ionization parameter. (5) Its covering fraction. (6) Photon index. (7) Cutoff energy. (8) Power-law normalization of the direct component. (9) Input soft photon temperature. (10) Plasma temperature. (11) Plasma optical depth. (12) Normalization. (13) Logarithmic ionization parameter of the accretion disk. (14) The inner radius of the disk. (15) Reflection strength. (16) Torus hydrogen column density along the equatorial plane. (17) Torus angular width. (18) Inclination angle. (19) Cross-calibration constant of *NuSTAR* relative to *XMM-Newton*/EPIC-PN. (20) Intrinsic luminosity in the 2–10 keV.

^aThe upper limit is pegged at the upper boundary value in the table model.

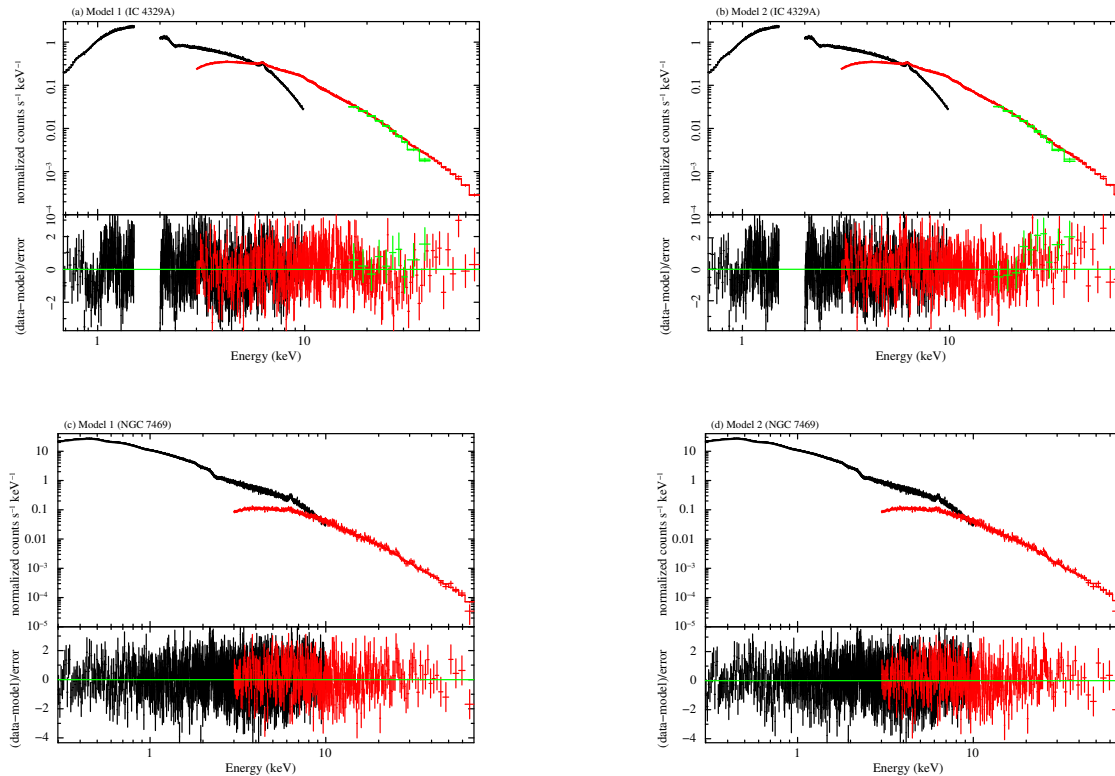


Figure 1. Observed broadband spectra of IC 4329A and NGC 7469 folded with the energy responses. The best-fit models are overplotted. Left: Model 1. Right: Model 2. upper: IC 4329A. Lower: NGC 7469. In the upper panels, the folded spectra of *Suzaku*/XIS (black crosses), *Suzaku*/HXD-PIN (green crosses), and *NuSTAR*/FPMs (red crosses) are plotted for IC 4329A, and those of *XMM-Newton*/EPIC-PN (black crosses) and *NuSTAR*/FPMs (red crosses) are plotted for NGC 7469. Solid curves represent the best-fit models. In the lower panels, the fitting residuals in units of 1σ error are shown.

absorbers) are often observed. In the iron-K band, in addition to a narrow Fe $K\alpha$ emission line centered at 6.4 keV, a broad emission line feature is sometimes recognized, although its intensity and shape strongly depend on the continuum modelling. The hard X-ray continuum shows a bump structure peaked around 30 keV over a power law component extrapolated from lower energies. The origins of these spectral features are still in debate, for which at least two distinct interpretations¹ have been proposed: (1) relativistically blurred reflection from the accretion disk (e.g., Tanaka et al. 1995), and (2) partial covering by line-of-sight absorbers with multiple ionization stages (e.g., Miyakawa et al. 2012).

We perform simultaneous fit to the *Suzaku*/XIS (0.7–10 keV), *Suzaku*/HXD-PIN (16–40 keV), and *NuSTAR*/FPMs (3–70 keV) data for IC 4329A, and *XMM-Newton*/EPIC-PN (0.3–10 keV) and *NuSTAR*/FPMs (3–70 keV) for NGC 7469. We ignore the 1.5–2.0 keV

range for IC 4329A to avoid possible calibration uncertainties in the *Suzaku*/XIS spectra.

The observed spectra folded with the energy responses are plotted in the upper panels of Figure 1(a)-(d).

Following major previous works, here we consider two spectral models: Model 1 where a relativistic reflection component from the accretion disk is included, for which we employ the RELXILL model (Dauser et al. 2013; García et al. 2014), and Model 2 where partial covering is applied to the direct component, for which we adopt the same model used by Iso et al. (2016). We consider warm absorber of one layer (Model 1) or two layers (Model 2). In both models, we utilize the XCLUMPY model to represent the reflection component (with fluorescence emission lines) from the torus. Model 1 and 2 are commonly applied to the spectra of both targets.

We always consider Galactic absorption, whose column density is fixed at the value estimated from the H I map by (Kalberla et al. 2005) for each target. To correct for relative calibration differences in the effective area among the instruments, we multiply a constant factor to the spectra. For IC 4329A, it is fixed at unity for

¹ Another interpretation considering dual power-law components have been proposed by e.g., Noda et al. (2013), see also Kawaguchi et al. (2001) for an earlier theoretical work.

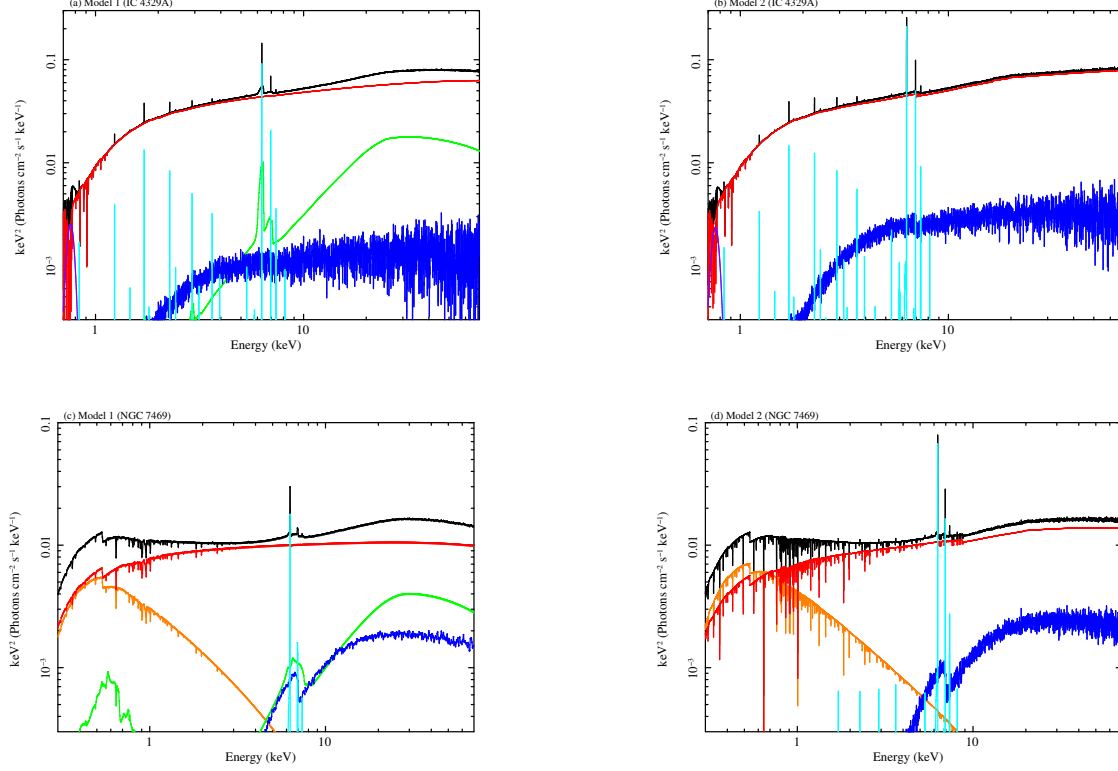


Figure 2. The best-fit models in units of $E I_E$ (where I_E is the energy flux at the energy E). Left: Model 1. Right: Model 2. upper: IC 4329A. Lower: NGC 7469. Black line: total. Red line: direct component. Green line: reflection component from the accretion disk. Blue line: reflection continuum from the torus. Light blue line: emission lines from the torus. Orange line: soft excess. Purple line: emission line at 0.77 keV.

Suzaku/XIS and at 1.16 for *Suzaku*/HXD-PIN (based on the calibration with the Crab Nebula), and is left free for *NuSTAR*/FPMs. For NGC 7469, it is fixed at unity for *XMM-Newton*/EPIC-PN and is left free for *NuSTAR*/FPMs.

4.1. Model 1: Relativistic Reflection Model

Model 1 is composed of a direct power-law component, its relativistic reflection component from the inner accretion disk, and that from the torus. The first two components are subject to a warm absorber in the line-of-sight. In the XSPEC terminology, the model is expressed as:

$$\begin{aligned}
 \text{Model 1} = & \text{const} * \text{phabs} \\
 & * (\text{zxcipcf} * (\text{zcutoffpl} + \text{compTT} + \text{relxill}) \\
 & + \text{atable}\{\text{xclumpy_R.fits}\} + \text{atable}\{\text{xclumpy_L.fits}\} \\
 & + \text{zgauss}).
 \end{aligned}
 \tag{1}$$

- (1) The `const` and `phabs` terms represent the cross-calibration constant and the Galactic absorption, respectively.
- (2) The `zcutoffpl` term represents the direct component (cutoff power-law), the `compTT` term the soft excess (thermal Comptonization model by Titarchuk 1994), and the `relxill` term the reflection component from the accretion disk based on the RELXILL code. All components are subject to absorption by a warm absorber (`zxcipcf`). The `compTT` term is required only in NGC 7469.

RELXILL is a state-of-art relativistic reflection model, which combines the XILLVER code (García et al. 2014), a reflection model from an ionized disk, with relativistic broadening by the RELLINE code (Dauser et al. 2010, 2013). The free parameters of RELXILL are the inclination angle of the observer with respect to the accretion disk (i), the iron abundance (Z_{Fe}), the photon index, the ionization parameter of the disk (ξ), the fraction of reflected flux ($R = \Omega/2\pi$, where Ω is the solid angle of the reflector), the spin param-

eter of the SMBH (a), the inner (q_1) and outer (q_2) emissivity indices, the radius at which the emissivity index changes (R_{br}), the inner (R_{in}) and outer (R_{out}) radii of the disk, and the cutoff energy. We assume $Z_{\text{Fe}} = 1.0$ (solar abundance), $q_1 = q_2 = 2.4$ (hence R_{br} is dummy), which is a mean value for local Seyfert 1 galaxies obtained by Patrick et al. (2012), and $R_{\text{out}} = 10^3 r_{\text{G}}$ (where r_{G} is the gravitational radius of the SMBH). We fix $a = 0$, which cannot be well constrained by the data. The inclination i is fixed at the value determined from the infrared data by Ichikawa et al. (2015). The photon index, normalization, and cutoff energy are linked to those of the `zcutoffpl` term.

- (3) The table models (`atable{xclumpy.R.fits}` and `atable{xclumpy.L.fits}`) correspond to the reflection continuum and emission lines from the torus, respectively, based on the XCLUMPY model. The parameters are the photon index, cutoff energy, equatorial hydrogen column density ($N_{\text{H}}^{\text{EQU}}$), torus angular width (σ), and inclination angle (i)². The photon index, normalization, and cutoff energy are linked to those of the `zcutoffpl` term. The values of σ and i are fixed at those determined from the infrared data by Ichikawa et al. (2015).
- (4) The `zgauss` term represents an emission line feature at 0.77 keV in IC 4329A (Brenneman et al. 2014).

We find that this model well reproduce the broadband spectra of both IC 4329A ($\chi^2/\text{dof} = 1338.8/1120$) and NGC 7469 ($\chi^2/\text{dof} = 1668.7/1574$). The best-fit parameters are summarized in the second columns of Tables 2 and 3, and the best-fit models folded with the responses and the fitting residuals are plotted in Figures 1(a) and 1(c) for IC 4329A and NGC 7469, respectively. The best-fit models in units of $EI(E)$, where I is the energy flux at the energy E , are plotted in Figures 2(a) and 2(c) for IC 4329A and NGC 7469, respectively.

4.2. Model 2: Partial Covering Model

As an alternative interpretation of X-ray spectra of Seyfert 1 galaxies to relativistic reflection models, Miyakawa et al. (2012) proposed the “variable partial

² The other parameters, the inner and outer radii of the torus, the radius of each clump, the number of clumps along the equatorial plane, and the index of radial density profile, are fixed at 0.05 pc, 1.00 pc, 0.002 pc, 10.0 and 0.50, respectively (Tanimoto et al. 2019).

covering” model and applied it for the spectral and timing analysis of MCG–6–30–15 (see also Miller et al. 2008 for an earlier work). In this model, the broad iron-K emission line feature is produced mainly by a deep iron K-edge structure due to the partial absorber in the line of sight. Iso et al. (2016) applied the same model to the *Suzaku* data of 20 nearby AGNs and found that it can reproduce the observations including time variability. Our Model 2, which is based on the model in Iso et al. (2016), is expressed in the XSPEC terminology as follows:

$$\begin{aligned} \text{Model 2} &= \text{const} * \text{phabs} \\ &* (\text{zxipcf} * \text{zxipcf} * (\text{zcutoffpl} + \text{compTT}) \\ &+ \text{atable}\{\text{xclumpy.R.fits}\} + \text{atable}\{\text{xclumpy.L.fits}\} \\ &+ \text{zgauss}). \end{aligned} \tag{2}$$

- (1) Same as Model 1-(1)
- (2) The `zcutoffpl` term represents the direct component and the `compTT` term the soft excess. Two layers of absorption by ionized matter (`zxipcf`) are multiplied, one of which is a partial absorber with a large column density ($N_{\text{H}} \sim 1 \times 10^{24} \text{cm}^{-2}$). Note that Miyakawa et al. (2012) considered three warm absorbers for MCG–6–30–15, whereas two are sufficient to explain our spectra of IC 4329A and NGC 7469.
- (3) Same as Model 1-(3)
- (4) Same as Model 1-(4)

We also find that Model 2 gives fairly good description of the broadband spectra for both targets ($\chi^2/\text{dof} = 1321.2/1120$ for IC 4329A and 1683.6/1574 for NGC 7469). Tables 2 and 3 (third columns) summarize the best-fit parameters, Figures 1(b) and 1(d) plot the best-fit folded models and the residuals, and Figures 2(b) and 2(d) plot the best-fit models in units of $EI(E)$ for IC 4329A and NGC 7469, respectively.

5. DISCUSSION

We have presented the results of our application of the X-ray clumpy torus model (XCLUMPY) to the broadband (0.3–70 keV) spectra of two seyfert 1 galaxies, IC 4329A and NGC 7469. This is the first work that utilizes the XCLUMPY model for type-1 AGNs. We find that both Model 1 (relativistic reflection model) and Model 2 (partial covering model) are able to reproduce the observed spectra almost equally well. This confirms

the degeneracy in interpreting the physical origins of the X-ray spectra of type-1 AGNs just by utilizing the time averaged spectroscopy. As mentioned in Section 1, we do not aim to favor or disfavor of either of the two interpretations in this paper. Below, we compare our results of the two models with previous works that adopted similar models (§ 5.1). Then, we discuss the torus properties of these AGNs by comparing our XCLUMPY results with the infrared results (§ 5.2), which is the main purpose of our work.

5.1. Comparison with Previous Studies

We have estimated realistic contribution of the reflection component from the torus in the broadband X-ray spectrum. The contribution to the total flux in the 10–50 keV band is found to be 1.8% (Model 1) and 4.5% (Model 2) for IC 4329A, and 11% (Model 1) and 14% (Model 2) for NGC 7469. In IC 4329A, we obtain a smaller $N_{\text{H}}^{\text{Equ}}$ value (hence a weaker intensity) with Model 1 than with Model 2. This is probably because a part of the narrow emission-line flux can also be accounted for by the emission line component in the RELXILL model under a limited energy resolution. A future high energy resolution spectroscopy, like that by *X-Ray Imaging and Spectroscopy Mission (XRISM)* and *Athena*, would help us separate the two components. In the case of NGC 7469, almost similar values are obtained with Models 1 and 2. In NGC 7469, the best-fit RELXILL model produces a much broader Fe K α line than that in the XCLUMPY model and hence such degeneracy is ignorable.

Previous works often utilized either `pexrav` or `pexmon` (Gondoin et al. 2001, Iso et al. 2016, and Miyake et al. 2016 for IC 4329A; Nandra et al. 2000 and Iso et al. 2016 for NGC 7469), or (unblurred) `xillver` with $\xi = 0$ (Brenneman et al. 2014 for IC 4329A; Middei et al. 2018 for NGC 7469) to represent the reflection component from distant matter or to approximate total reflection components including that from the accretion disk. A notable difference is that XCLUMPY with $N_{\text{H}}^{\text{Equ}} \leq 10^{24} \text{ cm}^{-2}$ produces a much weaker reflection hump at ~ 30 keV because the reflector is not as optically thick as assumed in `pexrav` or `xillver`. In fact, when we replace XCLUMPY with `pexmon`³ in our models, the flux of the torus reflection component at 30 keV is increased by a factor of 5.0 for IC 4329A and by 2.0 for NGC 7469 compared with the case of XCLUMPY.

³ In the spectral fit the inclination is fixed at 60 degrees, the photon index and cutoff energy are linked to those in the direct component, and the reflection strength $\Omega/2\pi$ (Ω is the solid angle of the reflector) is set free.

It inevitably affects estimates of the other spectral parameters. Thus, it is very important to adopt a realistic model for the torus reflection for correctly interpreting the broadband X-ray spectra of AGNs.

In Model 1 we consider two reflection components, one from the torus and the other from the inner accretion disk utilizing the RELXILL code. Our model yields $R_{\text{in}} = 87_{-31}^{+73} r_{\text{G}}$ for IC 4329A, and $R_{\text{in}} = 9.4_{-3.4}^{+26} r_{\text{G}}$ for NGC 7469, by assuming the emissivity index $q = 2.4$, the spin parameter $a = 0$ and the inclination angle (i) determined by the infrared data. This would suggest that the accretion disk in IC 4329A is truncated before reaching the innermost stable orbit (ISCO), supporting the argument by Done et al. (2000). By contrast, our result is consistent with the disk in NGC 7469 extending to the ISCO (i.e., $6 r_{\text{G}}$ for $a = 0$); this conclusion does not change even if we adopt $a = 0.998$ (maximum spin) instead. Patrick et al. (2012) applied the `relline` model, the same code as in RELXILL, to the *Suzaku* and *Swift*/BAT spectra of nearby Seyfert 1s including our targets. Although direct comparison is difficult because of parameter coupling (they made q and i free but fixed either a or R_{in}), their results are also consistent with a truncated disk in IC 4329A ($R_{\text{in}} = 37_{-9}^{+8} r_{\text{G}}$, $a = 0.998$ (fixed), $q = 2.3_{-0.4}^{+0.3}$, and $i = 51_{-3}^{+4}$ degrees) and with a disk extending to the ISCO in NGC 7469 ($R_{\text{in}} = R_{\text{ISCO}}$, $a = 0.78_{-0.17}^{+0.18}$, $q = 1.7_{-0.8}^{+0.1}$, and $i = 80_{-5}^{+8}$ degrees, where R_{ISCO} is the radius of the ISCO).

In Model 2, we confirm the claim by Iso et al. (2016) that a partial covering model with a large column density of $N_{\text{H}} \sim 10^{24} \text{ cm}^{-2}$ can reproduce the data without invoking a relativistic reflection from the accretion disk. The best-fit column density and ionization parameter of the absorbers are not exactly the same as those in Iso et al. (2016): they obtained $N_{\text{H},2} = 1.62_{-0.07}^{+0.27} \times 10^{24} \text{ cm}^{-2}$ and $\log \xi_2 = 1.49_{-0.52}^{+0.23}$ for IC 4329A and $N_{\text{H},2} = 1.64_{-0.28}^{+1.06} \times 10^{24} \text{ cm}^{-2}$ and $\log \xi_2 = 1.42_{-0.44}^{+0.58}$ for NGC 7469 (their Table 2) and a full absorber (ZX-IPCF1) is not required in both targets. The discrepancy is probably because we utilized a simplified `zxcipcf` model, whereas Iso et al. (2016) utilized their own XSTAR based warm absorber model. Also, the difference between XCLUMPY and `pexrav`, which is utilized by Iso et al. (2016), could affect the fit. Application of more sophisticated absorption models utilizing XSTAR is beyond the scope of this paper.

5.2. Comparison with the Infrared Results

In a type-1 AGN that shows no line-of-sight absorption, the equivalent width of a narrow iron K α line carries key information on the torus parameters assuming that the contributions to the line flux from the outer

accretion disk and/or BLR are unimportant. There is, however, degeneracy among the parameters, $N_{\text{H}}^{\text{Equ}}$, σ , and i (see Appendix). To avoid it, we have fixed σ and i at the values obtained from the infrared observations by [Ichikawa et al. \(2015\)](#). This enables us to make direct comparison on $N_{\text{H}}^{\text{Equ}}$ with the infrared results. While X-rays measure all material (gas and dust) among which gas is dominant in mass, infrared data are only sensitive to the amount of dust. Thus, we can constrain the gas-to-dust ratio (in terms of the ratio between the optical extinction and the X-ray column density) in the torus. In this analysis, it is implicitly assumed that the gas and dust have the same spatial distribution.

[Ichikawa et al. \(2015\)](#) determined the V-band extinction along the equatorial plane to be $A_{\text{V}} = 1.93 \pm 0.17 \times 10^3$ mag for IC 4329A and $A_{\text{V}} = 1.75_{-0.33}^{+0.30} \times 10^3$ mag for NGC 7469. Combining the X-ray results of $N_{\text{H}}^{\text{Equ}}$ with these A_{V} values, we derive the $N_{\text{H}}/A_{\text{V}}$ ratios to be $(2.8\text{--}7.4) \times 10^{19} \text{ cm}^{-2} \text{ mag}^{-1}$ (IC 4329A) and $(4.7\text{--}8.2) \times 10^{20} \text{ cm}^{-2} \text{ mag}^{-1}$ (NGC 7469), which are smaller than the canonical value of Galactic ISM, $1.87 \times 10^{21} \text{ cm}^{-2} \text{ mag}^{-1}$ ([Draine 2003](#)), by factors of 25–68 and 2.3–3.9 for IC 4329A and NGC 7469, respectively; when we compare our results with those obtained by [Maiolino et al. \(2001\)](#), the differences are further enhanced by factors of $\sim 3\text{--}100$. This result suggests that their tori are more “dusty” than, or have different dust properties (e.g., size distribution) from Galactic ISM.

To confirm this trend in an alternative way, we also perform spectral analysis by fixing $N_{\text{H}}^{\text{Equ}}$ at the infrared results (converted with the Galactic $N_{\text{H}}/A_{\text{V}}$ ratio) and leaving σ free. Then, we obtain $\sigma \leq 10.1$ degrees (Model 1,2)⁴ for IC 4329A, and $\sigma = 17.8_{-6.2}^{+3.0}$ degrees (Model 1) and $\sigma = 20.0_{-3.0}^{+0.8}$ degrees (Model 2) for NGC 7469. These σ values are smaller than the infrared results, 40 ± 1 degrees (IC 4329A) and 21 ± 2 degrees (NGC 7469). In this picture, the gas-to-dust ratio is the same as the Galactic ISM one at the equatorial plane but rapidly decreases with the elevation angle (i.e., the dust is vertically more extended than the gas), making the “averaged” gas-to-dust ratio in the torus smaller than the Galactic value.

On the basis of the X-ray results on σ , it is possible to infer the covering fraction of the torus (with $N_{\text{H}} > 10^{22} \text{ cm}^{-2}$), C_{T} . In XCLUMPY, the mean hydrogen column density at the elevation angle $\theta (\equiv 90^\circ - i)$ is given by

$$N_{\text{H}}(\theta) = N_{\text{H}}^{\text{Equ}} \exp\left(-\left(\frac{\theta}{\sigma}\right)^2\right). \quad (3)$$

⁴ The lower limit is pegged at 10 degrees (the lower boundary value in the table model).

Defining θ_{c} such that $N_{\text{H}}(\theta_{\text{c}}) = 10^{22} \text{ cm}^{-2}$, we find $\theta_{\text{c}} \leq 24.5$ degrees and $\theta_{\text{c}} = 27.9\text{--}50.0$ degrees, which corresponding to $C_{\text{T}} \leq 0.41$ and $C_{\text{T}} = 0.47\text{--}0.77$ for IC 4329A and NGC 7469, respectively. We can compare these values with the predictions from [Ricci et al. \(2017\)](#), who showed that the Eddington ratio λ_{Edd} is the key parameter that determines the torus geometry. At $\lambda_{\text{Edd}} = 0.13\text{--}0.16$ (for IC 4329A) and $\lambda_{\text{Edd}} = 0.36\text{--}0.40$ (for NGC 7469),⁵ the mean torus covering fractions are predicted to be $\sim 0.22\text{--}0.44$ and $\sim 0.22\text{--}0.42$, respectively ([Ricci et al. 2017](#)). Our result for IC 4329A is consistent with this prediction, whereas that for NGC 7469 is larger than it. We might be overestimating the torus reflection component in NGC 7469 because of possible contributions from the outer accretion disk and/or BLR in the observed iron-K line flux. Even if it is the case, it strengthens our conclusion that the torus is dusty.

Our results suggest that at least a non-negligible fraction of AGNs have more “dusty” torus than Galactic ISM. This argument may seem to be opposite to the well-known previous results reporting larger $N_{\text{H}}/A_{\text{V}}$ values than in Galactic ISM in some AGNs (e.g., [Maiolino et al. 2001](#)). However, we note that the sample of [Maiolino et al. \(2001\)](#) is not an unbiased one but is consisting of AGNs that show cold absorption in X-rays and optical broad emission lines. On the basis of the “dust color” method to measure optical extinction, [Burtscher et al. 2016](#) showed that $N_{\text{H}}/A_{\text{V}}$ values were on average consistent with the Galactic value when variability in N_{H} due to dust-free gas in the BLR is considered, except for heavily obscured AGNs. In fact, by applying the XCLUMPY model to 12 obscured AGNs in the [Ichikawa et al. \(2015\)](#) sample, [Tanimoto et al. \(in prep.\)](#) report that the mean value of $N_{\text{H}}/A_{\text{V}}$ in the line-of-sight material is similar to the Galactic ISM value, although there is a large scatter (~ 1 dex) among the sample. The reason behind the variation in $N_{\text{H}}/A_{\text{V}}$ among individual objects is unclear. The mid-infrared to X-ray luminosity ratios of IC 4329A and NGC 7469 are located close to the standard correlation ([Ichikawa et al. 2019](#)), apparently implying that the total amounts of dust are not largely different from other AGNs. Further systematic studies using a larger sample would be required to solve this issue.

6. CONCLUSION

⁵ Here we adopt the black hole masses $M_{\text{BH}} = 1.2 \times 10^8 M_{\odot}$ for IC 4329A ([de La Calle Pérez et al. 2010](#)) and $M_{\text{BH}} = 1.1 \times 10^7 M_{\odot}$ for NGC 7469 ([Peterson et al. 2014](#)), and convert the 2–10 keV luminosities to bolometric ones with a correction factor of 30.

In this paper, we have reported the application of the X-ray clumpy torus model XCLUMPY to the broadband spectra of two Seyfert 1 galaxies, IC 4329A and NGC 7469, whose torus parameters were obtained from the infrared spectra (Ichikawa et al. 2015). This is the first work that utilizes XCLUMPY for unobscured AGNs. We have shown that the intensity of the narrow Fe K α fluorescence line can be used to infer the torus geometry, even in type-1 AGNs that show no line-of-sight absorption. The main conclusions are summarized below.

1. We are able to well produce the simultaneously observed broadband (0.3–70 keV) spectra of both targets with two different models containing XCLUMPY: (Model 1) a relativistic reflection model and (Model 2) partial covering model. By fixing the angular width and inclination at the values determined by the infrared spectra, we constrain the column density along the equatorial plane for each object.
2. The XCLUMPY component (i.e., the torus reflection component) produces a weaker hump structure at ~ 30 keV compared with other reflection models such as `pexmon` and `xillver`. This fact must be correctly taken into account when interpreting AGN broadband spectra.
3. By comparing with the infrared results, the $N_{\text{H}}/A_{\text{V}}$ ratios are found to be by factors of 25–68 and 2.3–3.9 smaller than the Galactic ISM value for IC 4329A and NGC 7469, respectively. This is opposite to the trend reported for some AGNs

(e.g., Maiolino et al. 2001). Our results suggest that a non-negligible fraction of AGNs have more “dusty” tori than Galactic ISM.

We thank the anonymous referee for a careful reading of our manuscript and comments that helped us to improve the quality of the paper. We thank Dr. Kohei Ichikawa for discussions. Part of this work was financially supported by the Grant-in-Aid for Scientific Research 17K05384 (Y.U.) and for JSPS fellows for young researchers (A.T.). This research has made use of the *NuSTAR* Data Analysis Software (NUSTAR-DAS) jointly developed by the ASI Science Data Center (ASDC, Italy) and the California Institute of Technology (Caltech, USA). This research also made use of data obtained with *XMM-Newton*, an ESA science mission with instruments and contributions directly funded by ESA Member States and NASA, and use of public *Suzaku* data obtained through the Data ARchives and Transmission System (DARTS) provided by the Institute of Space and Astronautical Science (ISAS) at the Japan Aerospace Exploration Agency (JAXA). For data reduction, we used software provided by the High Energy Astrophysics Science Archive Research Center (HEASARC) at NASA/Goddard Space Flight Center.

Facilities: *XMM-Newton*, *Suzaku*, *NuSTAR*.

Software: HEASoft (HEASARC 2014), SAS (v17.0.0; Gabriel et al. 2004), NUSTARDAS, XSPEC (Arnaud 1996), RELXILL (Dauser et al. 2013; García et al. 2014), XCLUMPY (Tanimoto et al. 2019).

APPENDIX

A. PREDICTED FE K α EQUIVALENT WIDTH FROM XCLUMPY FOR UNOBSERVED AGNS

Using XCLUMPY model, we investigate dependences of predicted iron-K equivalent width on torus parameters: hydrogen column density along the equatorial plane ($N_{\text{H}}^{\text{Equ}}$), torus angular width (σ), and inclination angle (i). Figure 3 plots the predicted iron-K equivalent width for type-1 AGNs as a function of the torus parameters.

REFERENCES

- Anders, E., & Grevesse, N. 1989, *Geochimica et Cosmochimica Acta*, 53, 197
- Arnaud, K. A. 1996, in *Astronomical Society of the Pacific Conference Series*, Vol. 101, *Astronomical Data Analysis Software and Systems V*, ed. G. H. Jacoby & J. Barnes, 17
- Barcons, X., Carrera, F. J., & Ceballos, M. T. 2003, *MNRAS*, 339, 757
- Beckmann, V., Gehrels, N., Shrader, C. R., & Soldi, S. 2006, *ApJ*, 638, 642
- Blustin, A. J., Branduardi-Raymont, G., Behar, E., et al. 2003, *A&A*, 403, 481
- Brenneman, L. W., Madejski, G., Fuerst, F., et al. 2014, *ApJ*, 788, 61
- Burtscher, L., Davies, R. I., Graciá-Carpio, J., et al. 2016, *A&A*, 586, A28

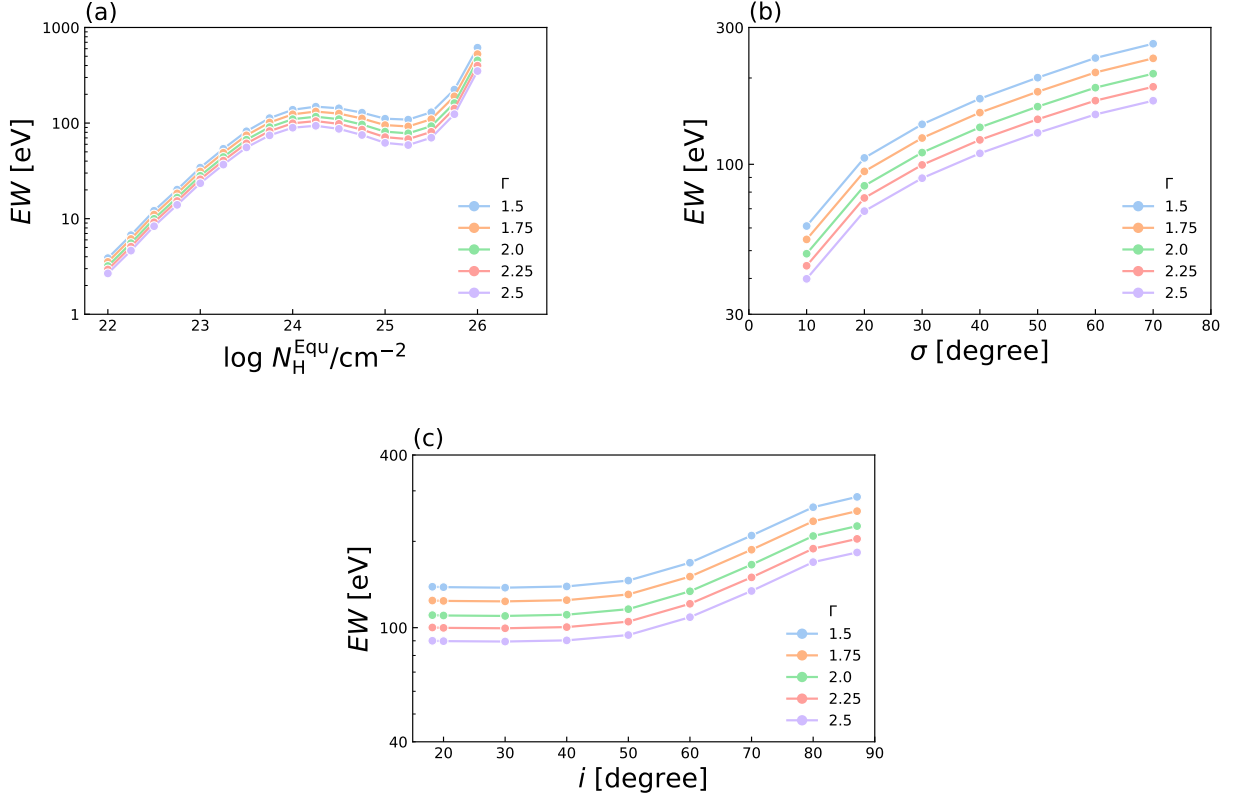


Figure 3. Predicted iron-K equivalent width for type-1 AGNs plotted as a function of torus parameter: (a) hydrogen column density along the equatorial plane, (b) torus angular width, and (c) inclination angle. Blue, orange, green, red, and violet lines correspond to photon indices of $\Gamma = 1.5, 1.75, 2.0, 2.25, 2.5$, respectively. We adopt $\log N_{\text{H}}^{\text{Equ}}/\text{cm}^{-2} = 24.0$, $\sigma = 30$ degrees, $i = 30$ degrees, and $E_{\text{Cut}} = 100$ keV. We note that the line-of-sight absorption is $\log N_{\text{H}} \sim 24$ in the case of $\log N_{\text{H}}^{\text{Equ}} \sim 26$.

Dauser, T., Garcia, J., Wilms, J., et al. 2013, MNRAS, 430, 1694
 Dauser, T., Wilms, J., Reynolds, C. S., & Brenneman, L. W. 2010, MNRAS, 409, 1534
 de La Calle Pérez, I., Longinotti, A. L., Guainazzi, M., et al. 2010, A&A, 524, A50
 De Rosa, A., Fabian, A. C., & Piro, L. 2002, MNRAS, 334, L21
 Done, C., Madejski, G. M., & Życki, P. T. 2000, ApJ, 536, 213
 Draine, B. T. 2003, Annual Review of Astronomy and Astrophysics, 41, 241
 Fukazawa, Y., Mizuno, T., Watanabe, S., et al. 2009, Publications of the Astronomical Society of Japan, 61, S17
 Gabriel, C., Denby, M., Fyfe, D. J., et al. 2004, in Astronomical Society of the Pacific Conference Series, Vol. 314, Astronomical Data Analysis Software and Systems (ADASS) XIII, ed. F. Ochsenbein, M. G. Allen, & D. Egret, 759
 García, J., Dauser, T., Lohfink, A., et al. 2014, ApJ, 782, 76

Gondoin, P., Barr, P., Lumb, D., et al. 2001, A&A, 378, 806
 González-Martín, O., Rodríguez-Espinosa, J. M., Díaz-Santos, T., et al. 2013, A&A, 553, A35
 Guainazzi, M., Matsuoka, M., Piro, L., Mihara, T., & Yamauchi, M. 1994, ApJ, 436, L35
 Harrison, F. A., Craig, W. W., Christensen, F. E., et al. 2013, ApJ, 770, 103
 Huang, X.-X., Wang, J.-X., Tan, Y., Yang, H., & Huang, Y.-F. 2011, ApJ, 734, L16
 Ichikawa, K., Packham, C., Ramos Almeida, C., et al. 2015, ApJ, 803, 57
 Ichikawa, K., Ricci, C., Ueda, Y., et al. 2019, ApJ, 870, 31
 Ishisaki, Y., Maeda, Y., Fujimoto, R., et al. 2007, Publications of the Astronomical Society of Japan, 59, 113
 Iso, N., Ebisawa, K., Sameshima, H., et al. 2016, Publications of the Astronomical Society of Japan, 68, S27
 Jansen, F., Lumb, D., Altieri, B., et al. 2001, A&A, 365, L1
 Kalberla, P. M. W., Burton, W. B., Hartmann, D., et al. 2005, A&A, 440, 775

- Kawaguchi, T., Shimura, T., & Mineshige, S. 2001, *ApJ*, 546, 966
- Kawamuro, T., Ueda, Y., Tazaki, F., Terashima, Y., & Mushotzky, R. 2016, *ApJ*, 831, 37
- Kokubun, M., Makishima, K., Takahashi, T., et al. 2007, *Publications of the Astronomical Society of Japan*, 59, 53
- Koyama, K., Tsunemi, H., Dotani, T., et al. 2007, *Publications of the Astronomical Society of Japan*, 59, 23
- Magdziarz, P., & Zdziarski, A. A. 1995, *MNRAS*, 273, 837
- Maiolino, R., Marconi, A., Salvati, M., et al. 2001, *A&A*, 365, 28
- McKernan, B., & Yaqoob, T. 2004, *ApJ*, 608, 157
- Middei, R., Bianchi, S., Cappi, M., et al. 2018, *A&A*, 615, A163
- Miller, L., Turner, T. J., & Reeves, J. N. 2008, *A&A*, 483, 437
- Mitsuda, K., Bautz, M., Inoue, H., et al. 2007, *Publications of the Astronomical Society of Japan*, 59, S1
- Miyakawa, T., Ebisawa, K., & Inoue, H. 2012, *Publications of the Astronomical Society of Japan*, 64, 140
- Miyake, K., Noda, H., Yamada, S., Makishima, K., & Nakazawa, K. 2016, *Publications of the Astronomical Society of Japan*, 68, S28
- Nandra, K., Le, T., George, I. M., et al. 2000, *ApJ*, 544, 734
- Nandra, K., O'Neill, P. M., George, I. M., & Reeves, J. N. 2007, *MNRAS*, 382, 194
- Nenkova, M., Sirocky, M. M., Ivezić, Ž., & Elitzur, M. 2008a, *ApJ*, 685, 147
- Nenkova, M., Sirocky, M. M., Nikutta, R., Ivezić, Ž., & Elitzur, M. 2008b, *ApJ*, 685, 160
- Noda, H., Makishima, K., Nakazawa, K., & Yamada, S. 2013, *ApJ*, 771, 100
- Odaka, H., Yoneda, H., Takahashi, T., & Fabian, A. 2016, *MNRAS*, 462, 2366
- Ordovás-Pascual, I., Mateos, S., Carrera, F. J., et al. 2017, *MNRAS*, 469, 693
- Patrick, A. R., Reeves, J. N., Porquet, D., et al. 2012, *MNRAS*, 426, 2522
- Peterson, B. M., Grier, C. J., Horne, K., et al. 2014, *ApJ*, 795, 149
- Ramos Almeida, C., & Ricci, C. 2017, *Nature Astronomy*, 1, 679
- Ricci, C., Ueda, Y., Ichikawa, K., et al. 2014, *A&A*, 567, A142
- Ricci, C., Trakhtenbrot, B., Koss, M. J., et al. 2017, *Nature*, 549, 488
- Risaliti, G., & Elvis, M. 2004, in *Astrophysics and Space Science Library*, Vol. 308, *Supermassive Black Holes in the Distant Universe*, ed. A. J. Barger, 187
- Risaliti, G., Elvis, M., Fabbiano, G., Baldi, A., & Zezas, A. 2005, *ApJ*, 623, L93
- Scott, J. E., Kriss, G. A., Lee, J. C., et al. 2005, *ApJ*, 634, 193
- Shu, X. W., Yaqoob, T., & Wang, J. X. 2010, *The Astrophysical Journal Supplement Series*, 187, 581
- Springob, C. M., Haynes, M. P., Giovanelli, R., & Kent, B. R. 2005, *The Astrophysical Journal Supplement Series*, 160, 149
- Steenbrugge, K. C., Kaastra, J. S., Sako, M., et al. 2005, *A&A*, 432, 453
- Strüder, L., Briel, U., Dennerl, K., et al. 2001, *A&A*, 365, L18
- Takahashi, T., Abe, K., Endo, M., et al. 2007, *Publications of the Astronomical Society of Japan*, 59, 35
- Tanaka, Y., Nandra, K., Fabian, A. C., et al. 1995, *Nature*, 375, 659
- Tanimoto, A., Ueda, Y., Odaka, H., et al. 2019, *ApJ*
- Tazaki, F., Ueda, Y., Terashima, Y., Mushotzky, R. F., & Tombesi, F. 2013, *ApJ*, 772, 38
- Titarchuk, L. 1994, *ApJ*, 434, 570
- Turner, M. J. L., Abbey, A., Arnaud, M., et al. 2001, *A&A*, 365, L27
- Vasudevan, R. V., Mushotzky, R. F., Winter, L. M., & Fabian, A. C. 2009, *MNRAS*, 399, 1553
- Willmer, C. N. A., Focardi, P., Chan, R., Pellegrini, P. S., & da Costa, N. L. 1991, *AJ*, 101, 57
- Winter, L. M., Mushotzky, R. F., Reynolds, C. S., & Tueller, J. 2009, *ApJ*, 690, 1322
- Yaqoob, T., & Warwick, R. S. 1991, *MNRAS*, 248, 773